frontiers | Frontiers in Physics

TYPE Original Research
PUBLISHED 22 December 2022
DOI 10.3389/fphy.2022.1111159

OPEN ACCESS

EDITED BY
Pei Li,
Xi'an Jiaotong University, China

REVIEWED BY
Yunfei Gao,
Hohai University, China
Chuang Lu,
University of Science and Technology of China, China

*CORRESPONDENCE
Xiaohui Yuan,
yxh@xynu.edu.cn

SPECIALTY SECTION
This article was submitted to Statistical and Computational Physics, a section of the journal Frontiers in Physics

RECEIVED 29 November 2022
ACCEPTED 12 December 2022
PUBLISHED 22 December 2022

CITATION
Li H, Zhao J, Guo X, Cheng Y, Xu Y and Yuan X (2022), Sensitivity analysis of flexoelectric materials surrogate model based on the isogeometric finite element method.
Front. Phys. 10:1111159.
doi: 10.3389/fphy.2022.1111159

Sensitivity analysis of flexoelectric materials surrogate model based on the isogeometric finite element method

Haozhi Li[1,2,3], Juan Zhao[1,2,3], Xiaokun Guo[1,2,3], Yu Cheng[1,2,3], Yanmin Xu[3,4] and Xiaohui Yuan[1,2,3]*

[1]College of Architecture and Civil Engineering, Xinyang Normal University, Xinyang, China, [2]Henan Unsaturated Soil and Special Soil Engineering Technology Research Center, Xinyang Normal University, Xinyang, China, [3]Henan International Joint Laboratory of Structural Mechanics and Computational Simulation, Huanghuai University, Zhumadian, China, [4]School of Architecture and Civil Engineering, Huanghuai University, Zhumadian, China

In this paper proposes a sensitivity analysis method based on a Polynomial Chaos Expansion (PCE) surrogate model for flexoelectric materials. The non-uniform rational B-splines (NURBS) basis functions to discretize the fourth-order partial differential equation for flexoelectricity and obtains a deterministic solution (electric potential). The mathematical expressions of surrogate model for the flexoelectric materials are established by considering uncertain parameters such as independent Young's modulus, concentrated load and flexoelectric constants. The sensitivity expression is found by derivation the mathematical expression for the surrogate model. Moreover the finite difference method (FDM) are conducted in numerical examples to demonstrate the validity and correctness of the proposed algorithm.

KEYWORDS

isogeometric analysis, polynomial chaos expansion, surrogate model, uncertainty quantification, sensitivity analysis

1 Introduction

Flexoelectricity is a new electromechanical energy conversion mechanism that can be an alternative to piezoelectricity [1]. The flexoelectricity is relatively weak in bulk crystalline materials, resulting in little attention. However, with the advancement of nanotechnology, huge strain gradients can be obtained at small-length scales, leading to a new understanding of the flexoelectricity as a size-dependent phenomenon [2]. As compared to piezoelectricity, flexoelectricity theoretically be present in all dielectrics, including those with centrosymmetric crystal structures, and is therefore a more versatile electromechanical coupling mechanism [3]. The traditional Lagrangian interpolation function of Finite Element Method (FEM) can only provide C^0 continuity requirements. The C^0 continuity of the FEM cannot satisfy the C^1 continuity requirement of the fourth-order partial differential equation for flexoelectricity. This requires other numerical methods to achieve the C^1 continuity requirement. Isogeometric analysis (IGA) is one

of the most popular numerical methods. It satisfies the continuity of C^1 by enhancing the order of NURBS basis function [4]. IGA initially developed to unify computer-aided design (CAD) and computer-aided engineering (CAE), but the remarkable characteristics of IGA basis functions such as NURBS has been applied to many applications including mechanics of fracture [5], electromagnetics [6], acoustics [7–10], and optimizations [11–14].

The input parameters of simulation models are often characterized by high uncertainty, and the model parameters are difficult and inaccurate to estimate [15]. This can largely lead us to make erroneous judgments about the issues of concern. The uncertainty quantification of input parameters is an efficient way to address uncertainty, and it examines the uncertainty in the model from the input parameters. Uncertainty analysis methods including Monte Carlo simulation (MCs) [16–18], the random spectral approach [19, 20] and the perturbation technique [21, 22] are frequently used to take into account the impact of uncertainty on the system response. However, with improving accuracy requirements, modeling of target simulation has become extremely complex, and its implementation is costly and time-consuming. The commonly used MCs approach is costly and challenging to implement for uncertainty quantification when many samples and model observations are required [23]. The surrogate modeling approach uses the relationship between inputs and outputs in a basic mathematical model to establish a new method for replacing complex analytical or computational models. The development of surrogate modeling techniques appropriate for solving practical engineering problems provides the required model observations and can reduce the computational cost of uncertainty quantification.

The Polynomial Chaos Expansion (PCE) becomes a prominent alternative modeling method in the field of uncertainty quantification (UQ) with low training cost when modeling extremely complex systems. The main implementation process of PCE is to use several polynomials to expand the response of random variables. The model response is expressed as a polynomial function of the input by determining the PCE coefficients of the polynomial components. These polynomial functions are orthogonal to the probability density functions of the input variables, which makes the calculation easier. The non-intrusive method does not require information about the control equations and is more suitable than the intrusive method for most problems when solving for the PCE coefficients. The non-intrusive methods include projection methods [24] and regression methods [25, 26] in which regression methods are more popular because of their efficiency in dealing with multivariate problems [27]. The sensitivity analysis (SA) quantitatively measures which the uncertainty of different input parameters contributes to the output uncertainty [28]. The sensitivity index is usually used to indicate the influence of each individual input parameter on the output [29]. Some complex problems in practical engineering do not have a definite input-output mathematical expression. It makes it difficult for engineers to perform sensitivity analysis on complex problems. The technique of surrogate modeling, such as PCE, can easily quantify the influence of the input parameters on the output by building mathematical expressions for the mechanical properties of complex problems depending on the inputs and outputs.

This paper lays out a procedure for solving the sensitivity problems of flexoelectric materials. This approach consists of two novel points:

1 The IGA-FEM and PCE are employed to establish a surrogate model for the flexoelectric materials.
2 The sensitivity expressions of the surrogate model are established by considering three kinds of different material parameters, respectively.

The remaining sections of the essay are structured as follows. The foundations of PCE in uncertainty quantification are presented in Section 2. Three introduces the principles of the isogeometric Finite Element Method for the statics of flexoelectric materials. Section 4 validates the IGA-FEM, PCE surrogate models and the sensitivity values of PCE surrogate models of the flexoelectric structure using numerical examples, followed by conclusions in Section 5.

2 Basic formula of polynomial chaos expansion

The basic idea of PCE is to replace the system model with an orthogonal polynomial defined by random variables, and then obtain a surrogate model expression by solving for the PCE coefficients. For the system model with n-dimensional independent random variables, the output function of the truncated PCE model with total expand order p can be expressed as

$$f(\mathbf{r}) = \sum_{\alpha}^{N-1} \theta_\alpha \Psi_\alpha(\mathbf{r}), \tag{1}$$

where the total number N of polynomial terms of order p is computed by $N = (n+p)!/(n!p!)$. θ_α are polynomial coefficients that are unknown. $\Psi_{\boldsymbol{\alpha}}$ are multivariate orthogonal polynomials defined by the tensor product of univariate orthogonal polynomials as

$$\Psi_\alpha(\mathbf{r}) = \prod_{i=1}^{n} \psi_{\alpha i}(r_i), \tag{2}$$

where $\psi_{\alpha i}(r_i)$ is a univariate polynomial with respect to the random variable r_i. The inner product of any two functions defined by $\Psi_s(\mathbf{r})$ and $\Psi_t(\mathbf{r})$, and the probability density function $P(\mathbf{r})$ of $\mathbf{r}$ is:

TABLE 1 The probability distributions of different random variables and corresponding orthogonal polynomials [4].

Distribution type of random variable	Orthogonal polynomials	Interval
Gamma	Laguerre	$(0, +\infty)$
Weibull		
Normal	Hermit	$(-\infty, +\infty)$
Uniform	Legendre	[a, b]
Beta	Jacobi	[a, b]
Poisson	Charlier	{0, 1, 2, . . ., }
Negative binomial	Meixner-Chaos	{0, 1, 2, . . ., }
Binomial	Krawtchouk	{0, 1, 2, . . ., n}
Hypergeometric	Hahn-Chaos	{0, 1, 2, . . ., n}

$$\langle \Psi_s(\mathbf{r}), \Psi_t(\mathbf{r}) \rangle = \int \Psi_s(\mathbf{r}) \Psi_t(\mathbf{r}) P(\mathbf{r}) \mathrm{d}\mathbf{r} = \delta_{st}, \tag{3}$$

where $\langle \cdot \rangle$ is the expectation operator. δ_{st} is the Kronecker symbol, which is equal to one when $s = t$ and otherwise zero.

In general, the probability density functions for different distributions correspond to different orthogonal polynomials, e.g., Legendre polynomials correspond to uniform distributions and Gaussian distributions correspond to Hermite polynomials. Table 1 lists the common univariate orthogonal polynomials and their corresponding probability distributions. There are various approaches to calculating the polynomial chaos expansion coefficient θ_α. The collocation method and the least-squares minimization problem are commonly employed to obtain the PCE coefficients. The orthogonal matrix and the PCE coefficient vector can be obtained according to Eq. 1 as [30].

$$\mathbf{\Psi} = \begin{bmatrix} \Psi_0(\mathbf{r}^1) & \dots & \Psi_{N-1}(\mathbf{r}^1) \\ \cdot & & \cdot \\ \cdot & & \cdot \\ \cdot & & \cdot \\ \Psi_0(\mathbf{r}^Z) & \dots & \Psi_{N-1}(\mathbf{r}^Z) \end{bmatrix} \quad \textbf{and} \quad \boldsymbol{\theta} = \begin{Bmatrix} \theta_0 \\ \cdot \\ \cdot \\ \cdot \\ \theta_{N-1} \end{Bmatrix}, \tag{4}$$

where Z is the number of random variables sample points. The PCE coefficient vector can be expressed as

$$\boldsymbol{\theta} = \left(\mathbf{\Psi}^{\mathrm{T}} \mathbf{\Psi}\right)^{-1} \mathbf{\Psi}^{\mathrm{T}} \mathbf{U}, \tag{5}$$

where $\mathbf{U} = \left\{ \{ f(\mathbf{r}) \}_{z=1}^{Z} \right\}^{\mathrm{T}}$. In this paper, an orthogonal polynomial with random variables satisfying a Gaussian distribution is used as an example. The recurrence relation for the Hermite orthogonal polynomials corresponding to the Gaussian distribution is

$$H_\alpha(r) = \frac{1}{(-1)^\alpha e^{-\frac{r^2}{2}}} \frac{d^\alpha}{dr^\alpha} \left[e^{-\frac{r^2}{2}} \right] = \alpha! \sum_{k=0}^{[\alpha/2]} (-1)^k \frac{1}{k! 2^k (\alpha - 2k)!} r^{\alpha - 2k}, \tag{6}$$

where $[\frac{\alpha}{2}]$ is an integer and less than or equal to $\frac{\alpha}{2}$ r denotes the random variable. The three-term recurrence equation for the Hermite orthogonal polynomial is expressed as

$$H_{\alpha+1}(r) = r H_\alpha(r) - \alpha H_{\alpha-1}(r). \tag{7}$$

The first six polynomials of $H_\alpha(r)$ are

$$\begin{aligned} &H_\alpha(r) = 1 \quad \alpha = 0, \\ &H_\alpha(r) = r \quad \alpha = 1, \\ &H_\alpha(r) = r^2 - 1 \quad \alpha = 2, \\ &H_\alpha(r) = r^3 - 3r \quad \alpha = 3, \\ &H_\alpha(r) = r^4 - 6r^2 + 3 \quad \alpha = 4, \\ &H_\alpha(r) = r^5 - 10r^3 + 15r \quad \alpha = 5. \end{aligned} \tag{8}$$

3 IGA discretization of the control equations for flexoelectricity

In this section, we summarize the controlling equations for dielectric solids considering the flexoelectric effect. More information see [31–33] and references included therein. The weak form of the flexoelectric control equation is

$$\begin{aligned} \int_\Omega \big(& C_{ijkl} \delta S_{ij} S_{kl} - e_{kij} E_k \delta S_{ij} - \mu_{lijk} E_l \delta S_{ij,k} - \kappa_{ij} \delta E_i E_j - e_{ikl} \delta E_i S_{kl} \\ & - \mu_{ijkl} \delta E_i S_{jk,l} \big) d\Omega - \int_{\Gamma_t} \bar{t}_i \delta u_i d\Gamma_t + \int_{\Gamma_D} \omega \delta \varphi d\Gamma_D = 0, \end{aligned} \tag{9}$$

where u_i denotes displacement; φ denotes the electric potential; C_{ijkl} represents the fourth-order elasticity tensor; the mechanical strain is denoted by S_{ij}, e_{ijk} is the third-order piezoelectric tensor, the electric field is defined as $E_i = -\varphi_i$; the fourth-order total flexoelectric tensor is denoted by μ_{ijkl}; κ_{ij} is dielectric tensor of second order; $\bar{t}_i$ denotes the mechanical traction; ω is surface charge density. The physical domain is denoted by Ω, with boundaries Γ_t and Γ_D corresponding to mechanical traction and electric displacements, respectively. In order to obtain the

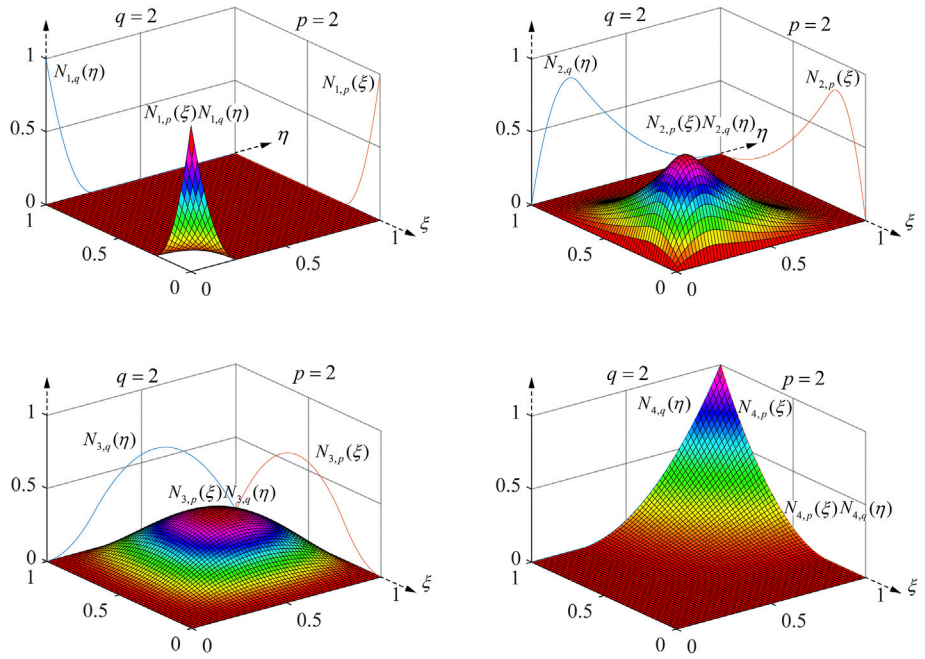

FIGURE 1
The specific B-spline basis functions.

FEM form of the governing Eq. 9, the B-spline basis function $N_{i,p}(\xi)$ obtained by recursively defining the Cox-de-Boor formula is

$$N_{i,0}(\xi) = \begin{cases} 1 & \text{if} \quad \xi_i \le \xi < \xi_{i+1} \\ 0 & \text{otherwise} \end{cases}, \tag{10}$$

and for $p = 1, 2, 3$,

$$N_{i,p}(\xi) = \frac{\xi - \xi_i}{\xi_{i+p} - \xi_i} N_{i,p-1}(\xi) + \frac{\xi_{i+p+1} - \xi}{\xi_{i+p+1} - \xi_{i+1}} N_{i+1,p-1}(\xi). \tag{11}$$

Figure 1 illustrates the results of visualizing the B-spline basis functions for both directional knot vectors with $\Xi^1 = [\,0 \quad 0 \quad 0 \quad 0.5 \quad 1 \quad 1 \quad 1\,]$ and $\Xi^2 = [\,0 \quad 0 \quad 0 \quad 0.5 \quad 1 \quad 1 \quad 1\,]$. The $N_{i,p}$ and $N_{i,q}$ are 2nd order basis functions. The richness of B-spline basis function can be intuitively seen in Figure 1. The richness of the basis functions provides the groundwork for solving the fourth-order partial differential equation for flexoelectricity. Using Eqs. 10, 11 to discretize Eq. 9, the linear algebraic system of equations for the flexoelectricity control equation is obtained as

$$\begin{bmatrix} \mathbf{A}_{uu} & \mathbf{A}_{u\varphi} \\ \mathbf{A}_{\varphi u} & \mathbf{A}_{\varphi\varphi} \end{bmatrix} \begin{bmatrix} \mathbf{u} \\ \Phi \end{bmatrix} = \begin{bmatrix} \mathbf{f}_u \\ \mathbf{f}_\varphi \end{bmatrix}, \tag{12}$$

where the matrix corresponding to the displacements is

$$\mathbf{A}_{uu} = \sum_e \int_{\Omega_e} (\mathbf{B}_u)^{\mathrm{T}} \mathbf{C} (\mathbf{B}_u) \mathrm{d}\Omega_e, \tag{13}$$

and

$$\mathbf{B}_u = \begin{bmatrix} \frac{\partial N_1}{\partial x} & \frac{\partial N_2}{\partial x} & \cdots & \frac{\partial N_{ncp}}{\partial x} & 0 & 0 & 0 & \cdots \\ 0 & 0 & \cdots & 0 & \frac{\partial N_1}{\partial y} & \frac{\partial N_2}{\partial y} & \cdots & \frac{\partial N_{ncp}}{\partial y} \\ \frac{\partial N_1}{\partial y} & \frac{\partial N_2}{\partial y} & \cdots & \frac{\partial N_{ncp}}{\partial y} & \frac{\partial N_1}{\partial x} & \frac{\partial N_2}{\partial x} & \cdots & \frac{\partial N_{ncp}}{\partial y} \end{bmatrix}, \tag{14}$$

$$\mathbf{C} = \left(\frac{Y}{(1+\nu)(1-2\nu)} \right) \begin{bmatrix} 1-\nu & \nu & 0 \\ \nu & 1-\nu & 0 \\ 0 & 0 & \left(\frac{1}{2} - \nu\right) \end{bmatrix}, \tag{15}$$

where ν is Poisson's ratio and Y is the Young's modulus. The matrix of displacement and electric field coupling are

$$\begin{aligned} \mathbf{A}_{u\varphi} &= \sum_e \int_{\Omega_e} \left[(\mathbf{B}_u)^{\mathrm{T}} \mathbf{e}^{\mathrm{T}} \left(\mathbf{B}_\varphi \right) + (\mathbf{H}_u)^{\mathrm{T}} \boldsymbol{\mu}^{\mathrm{T}} \left(\mathbf{B}_\varphi \right) \right] \mathrm{d}\Omega_e, \\ \mathbf{A}_{\varphi u} &= \sum_e \int_{\Omega_e} \left[\left(\mathbf{B}_\varphi \right)^{\mathrm{T}} \mathbf{e} (\mathbf{B}_u) + \left(\mathbf{B}_\varphi \right)^{\mathrm{T}} \boldsymbol{\mu} (\mathbf{H}_u) \right] \mathrm{d}\Omega_e. \end{aligned} \tag{16}$$

The electric field and Hessian matrices are

$$\mathbf{B}_{\varphi} = \begin{bmatrix} \frac{\partial N_1}{\partial x} & \cdots & \frac{\partial N_{ncp}}{\partial x} \\ \frac{\partial N_1}{\partial y} & \cdots & \frac{\partial N_{ncp}}{\partial y} \end{bmatrix},$$

$$\mathbf{H}_{u} = \begin{bmatrix} \frac{\partial^2 N_1}{\partial x^2} & \frac{\partial^2 N_2}{\partial x^2} & \cdots & \frac{\partial^2 N_{ncp}}{\partial x^2} & 0 & 0 & \cdots & 0 \\ 0 & 0 & \cdots & 0 & \frac{\partial^2 N_1}{\partial y \partial x} & \frac{\partial^2 N_2}{\partial y \partial x} & \cdots & \frac{\partial^2 N_{ncp}}{\partial y \partial x} \\ \frac{\partial^2 N_1}{\partial y \partial x} & \frac{\partial^2 N_2}{\partial y \partial x} & \cdots & \frac{\partial^2 N_{ncp}}{\partial y \partial x} & \frac{\partial^2 N_1}{\partial x^2} & \frac{\partial^2 N_2}{\partial x^2} & \cdots & \frac{\partial^2 N_{ncp}}{\partial x^2} \\ \frac{\partial^2 N_1}{\partial x \partial y} & \frac{\partial^2 N_2}{\partial x \partial y} & \cdots & \frac{\partial^2 N_{ncp}}{\partial x \partial y} & 0 & 0 & \cdots & 0 \\ 0 & 0 & \cdots & 0 & \frac{\partial^2 N_1}{\partial y^2} & \frac{\partial^2 N_2}{\partial y^2} & \cdots & \frac{\partial^2 N_{ncp}}{\partial y^2} \\ \frac{\partial^2 N_1}{\partial y^2} & \frac{\partial^2 N_2}{\partial y^2} & \cdots & \frac{\partial^2 N_{ncp}}{\partial y^2} & \frac{\partial^2 N_1}{\partial x \partial y} & \frac{\partial^2 N_2}{\partial x \partial y} & \cdots & \frac{\partial^2 N_{ncp}}{\partial x \partial y} \end{bmatrix}, \tag{17}$$

The piezoelectric constants and flexoelectric constants matrices are

$$\mathbf{e} = \begin{bmatrix} 0 & 0 & e_{115} \\ e_{311} & e_{333} & 0 \end{bmatrix},$$

$$\boldsymbol{\mu} = \begin{bmatrix} \mu_{11} & \mu_{12} & 0 & 0 & 0 & \mu_{44} \\ 0 & 0 & \mu_{44} & \mu_{12} & \mu_{11} & 0 \end{bmatrix}. \tag{18}$$

The matrix corresponding to the electric field is

$$\mathbf{A}_{\varphi\varphi} = -\sum_{e} \int_{\Omega_e} \left(\mathbf{B}_{\varphi}\right)^{\mathrm{T}} \boldsymbol{\kappa} \left(\mathbf{B}_{\varphi}\right) \mathrm{d}\Omega_e, \tag{19}$$

where the permittivity constant matrix is

$$\boldsymbol{\kappa} = \begin{bmatrix} \kappa_{11} & 0 \\ 0 & \kappa_{22} \end{bmatrix}. \tag{20}$$

The force and electrical load vectors are

$$\begin{aligned} \mathbf{f}_u &= \sum_{e} \int_{\Gamma_{te}} \mathbf{N}_u{}^{\mathrm{T}} \mathbf{t}_{\Gamma} \mathrm{d}\Gamma_{te}, \\ \mathbf{f}_{\varphi} &= -\sum_{e} \int_{\Gamma_{De}} \mathbf{N}_{\varphi}{}^{\mathrm{T}} \omega \mathrm{d}\Gamma_{De}, \end{aligned} \tag{21}$$

The subscript e in Ω_e, Γ_{te} and Γ_{De} represents the eth finite element in Eqs. 13, 16, 19, 21.

4 Numercial examples

In this section, we verify the accuracy of the IGA-FEM for solving the fourth-order partial differential equation using a benchmark example of a cantilever beam. After that, some random variable sample points are selected to obtain the output of IGA-FEM, which is used to build a polynomial chaos expansion surrogate model. Finally, the sensitivity results of the surrogate model for the mechanical properties of flexoelectric materials are verified by several numerical examples. For the cantilever beam model, we postulate that the model satisfies plane strain linear elastic isotropy.

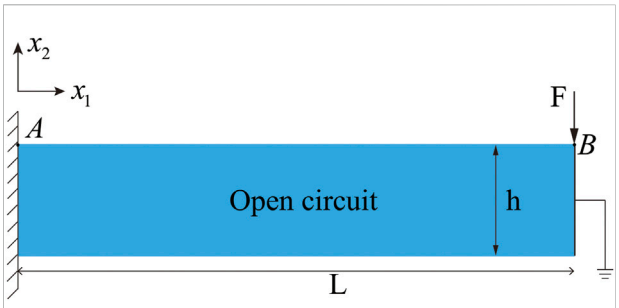

FIGURE 2
Cantilever beam model with open circuit electric boundary conditions.

TABLE 2 Material parameters for cantilever beam.

Name	$BaTiO_3$
Beam aspect ratio L/h	30
Poisson ratio ν	0.35
Young's modulus Y	120 Gpa
Piezoelectric constant e_{311}	−4.3 C/m^2
Flexoelectric constant ν_{12}	1.2 μC/m
Dielectric constants	
κ_{11}	9.9 nC/(Vm)
κ_{33}	11.2 nC/(Vm)
Electric susceptibility χ_{33}	1,408
Concentrated load F	200 μN

4.1 Model verification

The cantilever beam model with open-circuit electrical boundary conditions and the top free edge subjected to a concentrated load of 200 μN is depicted in Figure 2. The most commonly used $BaTiO_3$ material was selected for the cantilever beam model, as summarized in Table 2. The mesh and control point information is demonstrated in Figure 3. The boundary condition of the cantilever beam potential is specified on the right side as 0 V. The FEM uses the traditional Lagrangian basis function, which requires a lot of meshing to achieve higher accuracy, but the processing efficiency is lower. However,

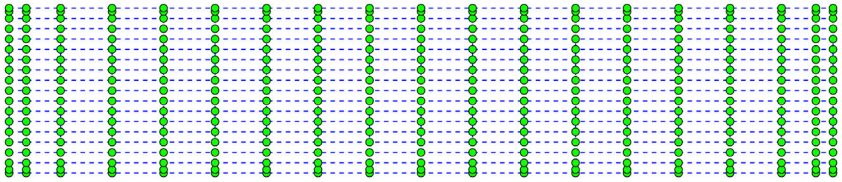

FIGURE 3
FEM discretization showing the control points as green dots.

TABLE 3 The normalized electromechanical coupling coefficient $\bar{\mathcal{K}}$ of non-piezoelectric materials with changing normalized thickness h'.

Non-piezoelectric materials			
Normalized thickness h'	IGA-FEM	Analytical solution	Relative error (%)
1	3.4642	3.4641	0.003
2	1.7323	1.7321	0.012
3	1.1549	1.1547	0.017
4	0.8662	0.866	0.023
5	0.6929	0.6928	0.014
6	0.5774	0.5774	0.000

IGA-FEM uses NURBS basis functions to reduce the preprocessing time by enhancing the order, which improves the computational efficiency. This is the main motivation for using IGA-FEM in this work.

The general definition of the electromechanical coupling coefficient $\mathcal{K}_{eff}$ is

$$\mathcal{K}_{eff} = \sqrt{\frac{\mathcal{W}_{elec}}{\mathcal{W}_{mech}}} = \sqrt{\frac{\int_{\Omega} {E_i}^{\mathrm{T}} \kappa_{ij} E \mathrm{d}\Omega}{\int_{\Omega} {S_{ij}}^{\mathrm{T}} C_{ijkl} S_{ij} \mathrm{d}\Omega}}, \tag{22}$$

For the one-dimensional cantilever beam problem, there are only stresses T_{11} and electric fields E_2 [31]. The electromechanical coupling coefficient of the cantilever beam problem is [34].

$$\mathcal{K}_{eff} = \frac{\chi_{33}}{1+\chi_{33}} \sqrt{\frac{\kappa_{33}}{Y}\left({e_{311}}^2 + 12\left(\frac{\mu_{12}}{h}\right)^2\right)}, \tag{23}$$

For comparison purposes, we introduce a normalized expression for the electromechanical coupling coefficient as

$$\bar{\mathcal{K}} = \frac{\mathcal{K}_{eff}}{\mathcal{K}_{\mathrm{piezo}}}, \tag{24}$$

and

$$\mathcal{K}_{\mathrm{piezo}} = \frac{\chi_{33}}{1+\chi_{33}} \sqrt{\frac{\kappa_{33}}{Y}{e_{311}}^2}. \tag{25}$$

The one-dimensional model can be obtained by setting the Poisson's ratio, the piezoelectric constant e_{333}, flexoelectric constant μ_{11} in the two-dimensional model to zero. The non-piezoelectric material is obtained by setting $e_{311} = 0$. The normalized electromechanical coupling coefficients obtained by IGA-FEM and analytical solutions are presented in Tables 3, 4. From the Tables 3, 4, it can be seen that the normalized electromechanical coupling coefficients obtained by IGA-FEM are very close to the analytical solution, and the relative errors are within a small range. The increase in standardized thickness will decrease the mechanical properties (electric potential) of the flexoelectric material.

4.2 PCE surrogate model verification

In this section, the output of the IGA-FEM of the cantilever beam model is used to build the PCE surrogate model. The Young's modulus, concentrated load and two flexoelectric constants as the random input variables are adopted, respectively. Table 5 lists the mean vlues, coefficients of variation, and ranges of sample points for the different random input variables. In this paper, we have used 500 sample points as input parameters for the random variables of the PCE. The Latin Hypercube Sampling (LHS) random number generation module in Matlab is utilized to obtain sample points of

TABLE 4 The normalized electromechanical coupling coefficient $\bar{K}$ of piezoelectric materials with changing normalized thickness h'.

Piezoelectric materials			
Normalized thickness h'	IGA-FEM	Analytical solution	Relative error (%)
1	3.5565	3.6056	1.36
2	1.9793	2.0000	1.04
3	1.5156	1.5275	0.78
4	1.3152	1.3229	0.58
5	1.2112	1.2166	0.44
6	1.1508	1.1547	0.34

TABLE 5 Definitions and the statistical characteristics of the random input variables.

Variables	Mean values $\mathcal{E}$	Coefficient of variation γ	The limits of variables: [lower, upper]
Young's modulus Y	120 GPa	0.1	[84,156]
Concentrated load F	200 μN	0.12	[128,272]
Flexoelectric constant μ_{11} / μ_{12}	1.2 μC/m	0.14	[0.7,1.7]

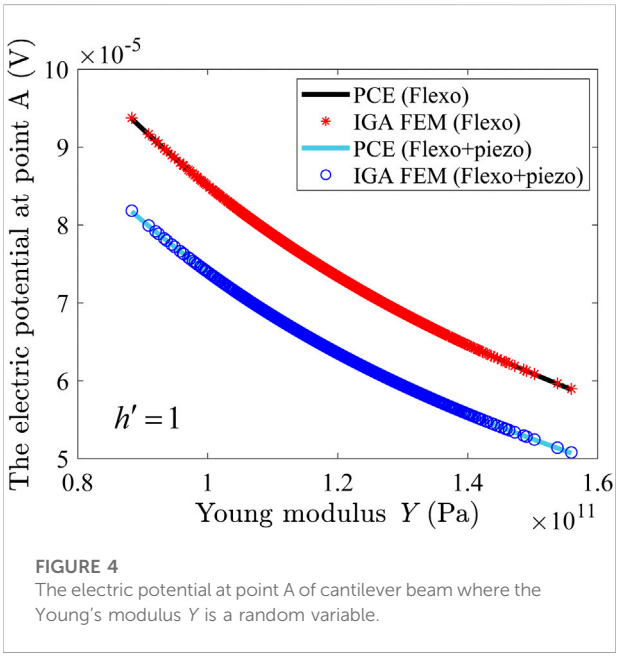

FIGURE 4
The electric potential at point A of cantilever beam where the Young's modulus Y is a random variable.

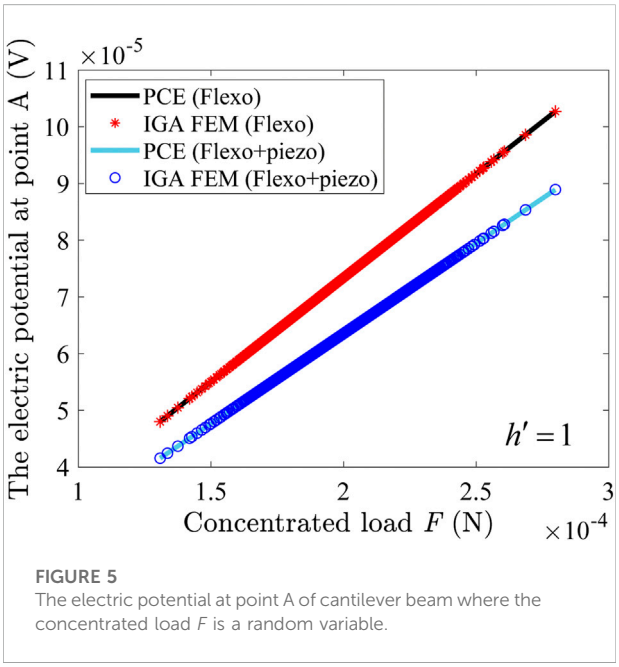

FIGURE 5
The electric potential at point A of cantilever beam where the concentrated load F is a random variable.

random variables. Owing to the potential distribution at the fixed edge is the most obvious, point A is selected as the reference point when establishing the surrogate model.

Figure 4 presents the comparison results of PCE and IGA-FEM for piezoelectric and non-piezoelectric materials with Young's modulus as random variable. As can be seen from Figure 4, the electric potential decreases as the Young's modulus increases. The PCE calculation results are basically consistent with the IGA-FEM calculation results, which verifies the effectiveness of the algorithm.

Figure 5 depicts the electric potential obtained by PCE and IGA-FEM for piezoelectric and non-piezoelectric materials with concentrated load as random variables. As can be seen from Figure 5, the electric potential of point A increases with increasing

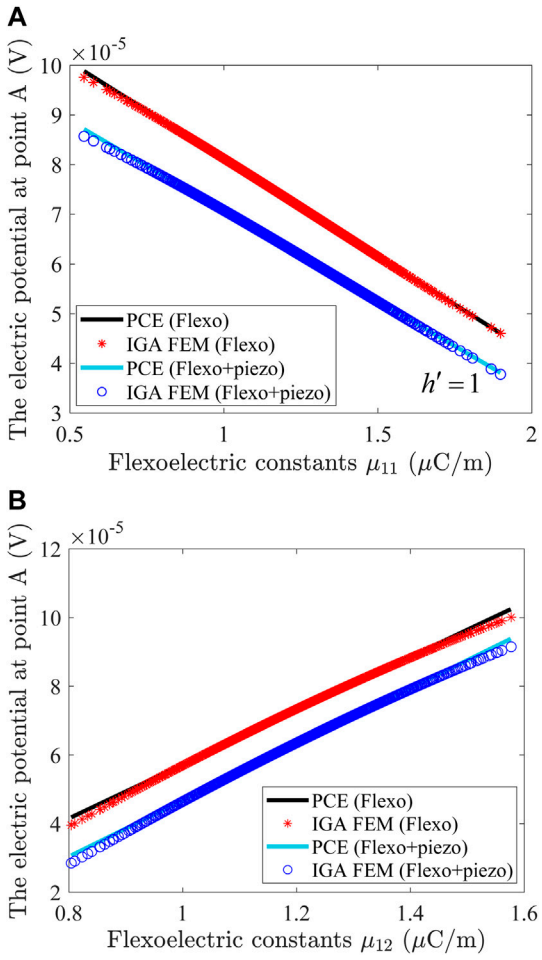

FIGURE 6
The electric potential at point A of the cantilever beam for different random variables. **(A)** The electric potential at point A of the cantilever beam when the random variable is μ_{11}. **(B)** The electric potential at point A of the cantilever beam when the random variable is μ_{12}.

concentrated load. The electric potential of a piezoelectric material subjected to the same concentrated force F is less than that of a non-piezoelectric material.

The results of PCE and IGA-FEM for piezoelectric and non-piezoelectric materials are shown in Figure 6, where the random variables are the flexoelectric constants μ_{11} and μ_{12}. It can be seen from Figure 6 that the electric potential presents reverse changes as the two different flexoelectric constants are changed.

4.3 Sensitivity analysis

In this section, we perform a sensitivity analysis of the surrogate model for the mechanical properties of flexoelectric materials obtained in Section 4.2. The sensitivity expression of the surrogate model for the mechanical properties of flexoelectric materials without considering piezoelectric effect are

$$\begin{aligned}
&\frac{d\Phi(Y)}{dY} = -2.42\times10^{-15} + 2.48\times10^{-26}Y - 7.35\times10^{-38}Y^2,\\
&\frac{d\Phi(F)}{dF} = 0.36697,\\
&\frac{d\Phi(\mu_{11})}{d\mu_{11}} = -39.0240,\\
&\frac{d\Phi(\mu_{12})}{d\mu_{12}} = 78.4851.
\end{aligned} \tag{26}$$

The sensitivity expression of the surrogate model for the mechanical properties of flexoelectric materials considering piezoelectric effect are

$$\begin{aligned}
&\frac{d\bar{\Phi}(Y)}{dY} = -2.24\times10^{-15} + 2.34\times10^{-26}Y - 6.99\times10^{-38}Y^2,\\
&\frac{d\Phi(F)}{dF} = 0.31776,\\
&\frac{d\bar{\Phi}(\mu_{11})}{d\mu_{11}} = -36.2533,\\
&\frac{d\bar{\Phi}(\mu_{12})}{d\mu_{12}} = 81.6950.
\end{aligned} \tag{27}$$

The sensitivity values obtained from the PCE surrogate model are compared with the global finite difference method (FDM) defined by

$$\frac{d\Phi(r)}{dr} = \frac{\Phi(r+\Delta r) - \Phi(r)}{\Delta r}. \tag{28}$$

To investigate the accuracy of DSM and FDM, one gives the relative error of DSM and FDM for different random variable r. The relative error of the sensitivity results obtained by FDM and PCE is

$$\epsilon_{err} = \frac{|\Phi_{PCE} - \Phi_{FDM}|}{|\Phi_{FDM}|}. \tag{29}$$

Owing to the first sensitivity expressions in Eqs. 27, 28 are a quadratic function of Young's modulus. Therefore, we need to calculate the sensitivity value of the surrogate model through the mean value of Young's modulus. The mean value of Young's modulus is lists in Table 5. The rest of the sensitivity values are directly selected from the derivative results. Tables 6, 7 present a comparison of the sensitivity values of PCE and FDM for non-piezoelectric and piezoelectric materials. From Tables 6, 7, it can be seen that the sensitivity values obtained by PCE and FDM are basically the same, and the relative errors are very small. In terms of the value of sensitivity, the flexoelectric constant μ_{12} has a greater effect on the electric potential of the flexoelectric material and the material is more sensitive to the flexoelectric constant μ_{12}.

TABLE 6 Comparison of PCE and FDM of sensitivity results for non-piezoelectric materials.

Non-piezoelectric			
Random variables	FDM	PCE	Relative error
Young's modulus Y	-5.04×10^{-16}	-5.01×10^{-16}	0.49%
Concentrated load F	0.36697	0.36697	-
Flexoelectric constant μ_{11}	−38.6675	−39.0240	0.9%
Flexoelectric constant μ_{12}	79.0227	78.4851	0.7%

TABLE 7 Comparison of PCE and FDM of sensitivity results for non-piezoelectric materials.

Piezoelectric			
Random variables	FDM	PCE	Relative error
Young's modulus Y	-4.48×10^{-16}	-4.46×10^{-16}	0.49%
Concentrated load F	0.31176	0.31176	-
Flexoelectric constant μ_{11}	−35.7991	−36.2533	1.3%
Flexoelectric constant μ_{12}	82.3133	81.6950	0.8%

5 Conclusion

In this paper, a sensitivity analysis method of surrogate model based on isogeometric stochastic Finite Element Method is proposed for flexoelectric materials. The NURBS basis functions with high-order continuity are used to discretize the fourth-order partial differential equation for flexoelectricity. The Polynomial Chaos Expansion (PCE) is utilized to develop a surrogate model for the mechanical properties of flexoelectric materials. The sensitivity values of the surrogate model are obtained by considering three kinds of different parameters, respectively. Numerical examples illustrate the flexoelectric material is more sensitive to the flexoelectric constant μ_{12}. Additionally, the current technology will also be used to three-dimensional piezoelectric and flexoelectric problems.

Data availability statement

The original contributions presented in the study are included in the article/Supplementary Material; further inquiries can be directed to the corresponding author.

Author contributions

Conceptualization, HL; Data curation, HL; Formal analysis, YC and YX; Investigation, XG; Methodology, HL and JZ; Project administration, XY, Software, HL and JZ; Supervision, XY; Validation, YX; Visualization, YC; Writing—original draft, HL and XG. All authors have read and agreed to the published version of the manuscript.

Conflict of interest

The authors declare that the research was conducted in the absence of any commercial or financial relationships that could be construed as a potential conflict of interest.

Publisher's note

References

1. Hamdia KM, Ghasemi H, Zhuang X, Alajlan N, Rabczuk T. Sensitivity and uncertainty analysis for flexoelectric nanostructures. *Comput Methods Appl Mech Eng* (2018) 337:95–109. doi:10.1016/j.cma.2018.03.016

2. Ahmadpoor F, Sharma P. Flexoelectricity in two-dimensional crystalline and biological membranes. *Nanoscale* (2015) 7:16555–70. doi:10.1039/C5NR04722F

3. Yudin PV, Tagantsev AK. Fundamentals of flexoelectricity in solids. *Nanotechnology* (2013) 24:432001. doi:10.1088/0957-4484/24/43/432001

4. Hughes TJ, Cottrell JA, Bazilevs Y. Isogeometric analysis: CAD, finite elements, NURBS, exact geometry and mesh refinement. *Comput Methods Appl Mech Eng* (2005) 194:4135–95. doi:10.1016/J.CMA.2004.10.008

5. Chen L, Wang Z, Peng X, Yang J, Wu P, Lian H. Modeling pressurized fracture propagation with the isogeometric BEM. *Geomechanics Geophys Geo-Energy Geo-Resources* (2021) 7:51. doi:10.1007/s40948-021-00248-3

6. Chen L, Lian H, Xu Y, Li S, Liu Z, Atroshchenko E, et al. Generalized isogeometric boundary element method for uncertainty analysis of time-harmonic wave propagation in infinite domains. *Appl Math Model* (2023) 114: 360–78. doi:10.1016/j.apm.2022.09.030

7. Chen L, Lu C, Lian H, Liu Z, Zhao W, Li S, et al. Acoustic topology optimization of sound absorbing materials directly from subdivision surfaces with isogeometric boundary element methods. *Comput Methods Appl Mech Eng* (2020) 362:112806. doi:10.1016/j.cma.2019.112806

8. Chen L, Lian H, Liu Z, Gong Y, Zheng C-J, Bordas S. Bi-material topology optimization for fully coupled structural-acoustic systems with isogeometric FEM-BEM. *Eng Anal Boundary Elem* (2022) 135:182–95. doi:10.1016/j.enganabound.2021.11.005

9. Chen L, Marburg S, Zhao W, Liu C, Chen H. Implementation of isogeometric fast multipole boundary element methods for 2d half-space acoustic scattering problems with absorbing boundary condition. *J Theor Comput Acoust* (2018) 27: 1850024. doi:10.1142/S259172851850024X

10. Chen L, Lu C, Zhao W, Chen H, Zheng C-J. Subdivision surfaces—boundary element accelerated by fast multipole for the structural acoustic problem. *J Theor Comput Acoust* (2020) 28:2050011. doi:10.1142/S2591728520500115

11. Chen L, Liu C, Zhao W, Liu L. An isogeometric approach of two dimensional acoustic design sensitivity analysis and topology optimization analysis for absorbing material distribution. *Comput Methods Appl Mech Eng* (2018) 336:507–32. doi:10.1016/j.cma.2018.03.025

12. Chen L, Lian H, Liu Z, Chen H, Atroshchenko E, Bordas S. Structural shape optimization of three dimensional acoustic problems with isogeometric boundary element methods. *Comput Methods Appl Mech Eng* (2019) 355:926–51. doi:10.1016/j.cma.2019.06.012

13. Chen L, Zhang Y, Lian H, Atroshchenko E, Ding C, Bordas SP. Seamless integration of computer-aided geometric modeling and acoustic simulation: Isogeometric boundary element methods based on catmull-clark subdivision surfaces. *Adv Eng Softw* (2020) 149:102879. doi:10.1016/j.advengsoft.2020.102879

14. Chen L, Lian H, Natarajan S, Zhao W, Chen X, Bordas S. Multi-frequency acoustic topology optimization of sound-absorption materials with isogeometric boundary element methods accelerated by frequency-decoupling and model order reduction techniques. *Comput Methods Appl Mech Eng* (2022) 395:114997. doi:10.1016/j.cma.2022.114997

15. Cheng K, Lu Z. Adaptive sparse polynomial chaos expansions for global sensitivity analysis based on support vector regression. *Comput Structures* (2018) 194:86–96. doi:10.1016/j.compstruc.2017.09.002

16. Hurtado J, Barbat A. Monte Carlo techniques in computational stochastic mechanics. *Arch Comput Methods Eng* (1998) 5:3–29. doi:10.1007/BF02736747

17. Chen L, Cheng R, Li S, Lian H, Zheng C, Bordas SP. A sample-efficient deep learning method for multivariate uncertainty qualification of acoustic–vibration interaction problems. *Comput Methods Appl Mech Eng* (2022) 393:114784. doi:10.1016/j.cma.2022.114784

18. Xu Y, Li H, Chen L, Zhao J, Zhang X. Monte Carlo based isogeometric stochastic finite element method for uncertainty quantization in vibration analysis of piezoelectric materials. *Mathematics* (2022) 10:1840. doi:10.3390/math10111840

19. Honda R. Stochastic BEM with spectral approach in elastostatic and elastodynamic problems with geometrical uncertainty. *Eng Anal Boundary Elem* (2005) 29:415–27. doi:10.1016/j.enganabound.2005.01.007

20. Liu WK, Belytschko T, Mani A. Random field finite elements. *Int J Numer Methods Eng* (1986) 23:1831–45. doi:10.1002/nme.1620231004

21. Kamiński M. Stochastic perturbation approach to engineering structure vibrations by the finite difference method. *J Sound Vibration* (2002) 251:651–70. doi:10.1006/jsvi.2001.3850

22. Kamiński M. On generalized stochastic perturbation-based finite element method. *Commun Numer Methods Eng* (2006) 22:23–31. doi:10.1002/cnm.795

23. Zhang B-Y, Ni Y-Q. A hybrid sequential sampling strategy for sparse polynomial chaos expansion based on compressive sampling and Bayesian experimental design. *Comput Methods Appl Mech Eng* (2021) 386:114130. doi:10.1016/j.cma.2021.114130

24. Le Maître O, Knio OM. *Spectral methods for uncertainty quantification: With applications to computational fluid dynamics*. Berlin, Germany: Springer Science & Business Media (2010).

25. Blatman G, Sudret B. Sparse polynomial chaos expansions and adaptive stochastic finite elements using a regression approach. *Comptes Rendus Mécanique* (2008) 336:518–23. doi:10.1016/j.crme.2008.02.013

26. Palar PS, Tsuchiya T, Parks GT. Multi-fidelity non-intrusive polynomial chaos based on regression. *Comput Methods Appl Mech Eng* (2016) 305:579–606. doi:10.1016/j.cma.2016.03.022

27. Zhou Y, Lu Z, Cheng K, Shi Y. An expanded sparse Bayesian learning method for polynomial chaos expansion. *Mech Syst Signal Process* (2019) 128:153–71. doi:10.1016/j.ymssp.2019.03.032

28. Saltelli A, Ratto M, Andres T, Campolongo F, Cariboni J, Gatelli D, et al. *Global sensitivity analysis: The primer*. New York, NY, USA: John Wiley & Sons (2008).

29. Hamdia KM, Silani M, Zhuang X, He P, Rabczuk T. Stochastic analysis of the fracture toughness of polymeric nanoparticle composites using polynomial chaos expansions. *Int J Fracture* (2017) 206:215–27. doi:10.1007/s10704-017-0210-6

30. Hauseux P, Hale JS, Bordas SP. Accelerating Monte Carlo estimation with derivatives of high-level finite element models. *Comput Methods Appl Mech Eng* (2017) 318:917–36. doi:10.1016/J.CMA.2017.01.041

31. Majdoub MS, Sharma P, Cagin T. Enhanced size-dependent piezoelectricity and elasticity in nanostructures due to the flexoelectric effect. *Phys Rev B* (2008) 77: 125424. doi:10.1103/PhysRevB.77.125424

32. Ghasemi H, Park HS, Rabczuk T. A level-set based Iga formulation for topology optimization of flexoelectric materials. *Comput Methods Appl Mech Eng* (2017) 313:239–58. doi:10.1016/j.cma.2016.09.029

33. Ghasemi H, Park HS, Alajlan N, Rabczuk T. A computational framework for design and optimization of flexoelectric materials. *Int J Comput Methods* (2020) 17: 1850097. doi:10.1142/S0219876218500974

34. Abdollahi A, Peco C, Millán D, Arroyo M, Arias I. Computational evaluation of the flexoelectric effect in dielectric solids. *J Appl Phys* (2014) 116:093502. doi:10.1063/1.4893974